A double-parabola model for the non-classical Cahn-Hilliard theory of homogeneous nucleation

1993 J. Phys.: Condens. Matter 5 7537

(http://iopscience.iop.org/0953-8984/5/41/002)

J. Phys.: Condens. Matter 5 (1993) 7537–7550. Printed in the UK

A double-parabola model for the non-classical Cahn–Hilliard theory of homogeneous nucleation

M Iwamatsu

Junior College of Management and Information Science, Chiba-Keizai University, 4-3-30 Todoroki-cho, Chiba 263, Japan

Received 29 March 1993, in final form 21 June 1993

Abstract. A double-parabola model is used to calculate various properties of the critical droplet in homogeneous nucleation using the Cahn–Hilliard non-classical theory, and the results are compared with those predicted from the classical theory due to Becker and Döring. The calculation can be performed mostly analytically, and various quantities can be characterized by two parameters: the supersaturation which measures difference in chemical potential from two-phase coexistence, and the asymmetry of thermodynamic properties of the liquid and the vapour phase. The predictions of the non-classical theory do not differ much from those of the classical theory in liquid–vapour nucleation (liquid droplet formation), but the difference is significant in vapour–liquid nucleation (gas bubble formation). In particular, the non-classical nucleation rate of bubble formation is found to be significantly faster, typically 18 orders of magnitude, than the classical nucleation rate. The deviations of the non-classical results from classical data increase as the asymmetry becomes more pronounced.

1. Introduction

Homogeneous nucleation [1,2], the formation of a critical droplet of a new phase, plays a central role in the understanding of the dynamics of every first-order phase transition, among which gas–liquid nucleation, the nucleation of liquid from supersaturated vapour, and its reverse process, liquid–gas nucleation, the nucleation of vapour bubbles from liquid under tensile stress (cavitation), are the oldest and the most famous examples. In the gas–liquid problem the 'classical nucleation theory' due to Volmer and Weber [3] and to Becker and Döring [4] is still a standard and usable theory, which is based on the transition state approach, in which the excess free energy $\Delta\Omega(R_0)$ of the critical droplet of liquid with the radius R_0 is regarded as an 'activation energy barrier' and the rate of nucleation of the critical droplet per unit volume and unit time has the form

$$J = J_0 \exp[-\Delta\Omega(R_0)/k_B T]. \tag{1.1}$$

The pre-exponential factor J_0 is calculated from the gas kinetic theory combined with a phenomenological sticking coefficient which describes the sticking probability of particles on the critical liquid droplet. This simple derivation of J_0 has been refined by Zeldvich [5] and by Langer and Turski [6] using more fundamental statistical approaches. However, the most important quantity of the theory is the energy barrier $\Delta\Omega(R_0)$, with which we shall be mainly concerned in this paper.

A central assumption of this 'classical' theory is known as the 'capillarity approximation', where even a small droplet is considered to be macroscopic, i.e. the inside

0953-8984/93/417537+14$07.50

of the droplet is a liquid with constant bulk density and thermodynamic properties, and the surface is infinitely narrow with the surface tension of a planar interface at two-phase coexistence; the effect of curvature on the surface and of inhomogeneity of density of the droplet are totally ignored. (A short review can be found in the paper of Oxtoby and Evans [7].) Using this approximation, the free-energy barrier in equation (1.1) consists of the free energy of bulk liquid inside the droplet and the surface free energy (tension) and is a function of the radius of the droplet:

$$\Delta\Omega(R) = -\tfrac{4}{3}\pi R^3|\Delta p| + 4\pi R^2\gamma. \tag{1.2}$$

The radius R_0 of the critical droplet is determined from the maximum $\partial(\Delta\Omega)/\partial R = 0$ as

$$R_0 = 2\gamma/|\Delta p| \tag{1.3}$$

where γ is the surface tension of the planar interface (at two-phase coexistence), and $\Delta p = p_v - p_l$ is the pressure difference between the centre of the liquid droplet and the (unstable) surrounding vapour. We note in passing that the same formula is applicable to liquid–gas nucleation where $p_l > p_v$, while $p_v > p_l$ in gas–liquid nucleation. Equation (1.3) is the so-called Laplace condition. Inserting equation (1.3) into equation (1.2), we find that the classical barrier height $\Delta\Omega_{cl} = \Delta\Omega(R_0)$ is given by

$$\Delta\Omega_{cl} = \tfrac{16}{3}\pi\gamma^3/(\Delta p)^2 \tag{1.4}$$

which is used to calculate the nucleation rate J in equation (1.1).

This classical theory can predict the nucleation rate J with reasonable accuracy for most substances [8], but recent more accurate measurements start to predict systematic deviations from the classical theory (see, e.g., [9, 10] and references cited in [1]). Cahn and Hilliard [11], furthermore, pointed out that this classical theory based on the capillarity approximation cannot predict the correct behaviour of the barrier height, which should vanish ($\Delta\Omega \to 0$) as the spinodal is approached and showed that 'non-classical nucleation theory' based on the square-gradient density-functional theory can predict this behaviour correctly. This 'non-classical' theory does not employ the capillarity approximation at all but calculates directly the free energy and the density profile of an inhomogeneous droplet as a function of supersaturation. Recently, Oxtoby and Evans [7] have extended the Cahn–Hilliard theory to the non-local van der Waals density functional with the Yukawa interaction; they also extended the theory to liquid–gas nucleation, the formation of bubbles in a liquid under negative pressure, and found a critical nucleation rate much larger (up to 19 orders of magnitude) than the prediction of classical theory. Zeng and Oxtoby [9] have applied this theory to a more realistic system with the Lennard-Jones interaction and found again a very large deviation from the classical theory.

This non-classical theory based on density-functional theory focuses primarily on the barrier height $\Delta\Omega$ and seems to cast doubt on the accuracy of the 'capillarity approximation'. Unfortunately, this conclusion is derived almost entirely from the results of numerical calculation and for specific models, and we cannot extract general conclusions except for special limiting cases; we have to repeat the numerical computation each time for specific materials. The purpose of this paper is to perform the calculation of this barrier height analytically as far as possible using the 'non-classical' Cahn–Hilliard theory combined with a double-parabola model for the free-energy density and obtain analytical relations between various quantities and, in particular, the dependence on supersaturation and on asymmetry between liquid and vapour phases.

The format of this paper is as follows. In section 2, we present the solution of the Cahn–Hilliard theory for the droplet using the double-parabola approximation and, in particular, the analytic solution for the density profile of the liquid droplet and the gas bubble. We calculate various quantities related to the critical droplet as a function of two parameters: the degree of supersaturation and the asymmetry of liquid and vapour. We conclude in section 4.

2. Formulation

According to density-functional theory, the density profile and the grand potential Ω of an inhomogeneous and non-equilibrium system such as a critical droplet away from coexistence are obtained from the saddle point in functional space of the grand potential density functional $\Omega[\rho(r)]$ and can be obtained by extremizing this functional by the density profile $\rho(r)$ [1, 2]. We consider the simplest square-gradient density functional originally employed by Cahn and Hilliard [10]. A grand potential functional of the critical droplet relative to unstable atmosphere is given by [1, 2]

$$\Delta\Omega[\rho(r)] = 4\pi \int_0^\infty \left[\omega(\rho) - \omega(\rho_b) + \tfrac{1}{2} L \left(\frac{d\rho}{dr} \right)^2 \right] r^2 \, dr \tag{2.1}$$

where

$$\omega(\rho) = f(\rho) - \mu\rho \tag{2.2}$$

is the grand potential density of a uniform system, and $f(\rho)$ represents the Helmholtz free energy density, μ is the chemical potential and L is the square-gradient coefficient. ρ_b is the density of the supersaturated vapour (in the case of liquid droplet formation) or the liquid under tensile force (in the case of cavitation). This square-gradient form is known to be a reasonable approximation for liquids interacting with a short-range force, but for liquids with a long-range algebraic force a more elaborate non-local density functional is necessary [12]. The relation between the square-gradient approximation and more complicated density-functional theories can be found in [13, 14].

The Euler–Lagrange equation, which determines the density profile

$$\delta\{\Delta\Omega[\rho(r)]\}/\delta\rho(r) = 0$$

is written as

$$d^2\rho/dr^2 + (2/r)(d\rho/dr) - (1/L)[\partial(\Delta\omega)/\partial\rho] = 0 \tag{2.3}$$

with

$$\Delta\omega(\rho) = \omega(\rho) - \omega(\rho_b). \tag{2.4}$$

This ordinary differential equation should be solved in conjunction with the boundary conditions

$$\begin{aligned} &(d\rho/dr)|_{r=0} = 0 \\ &\rho(r = \infty) = \rho_b. \end{aligned} \tag{2.5}$$

We shall adopt the double-parabola model (figure 1) for the free-energy density $\omega(\rho)$, which is frequently used in the square-gradient Landau-type theory as well as in the more sophisticated non-local van der Waals-type theory not too close to the critical point [15–18]:

$$\omega(\rho) = \begin{cases} \frac{1}{2}L\lambda_v^2(\rho - \rho_{v0})^2 - L\,\Delta\mu\,\rho & \rho < \rho_m \\ \frac{1}{2}L\lambda_l^2(\rho - \rho_{l0})^2 - L\,\Delta\mu\,\rho & \rho > \rho_m \end{cases} \tag{2.6}$$

where $L\,\Delta\mu$ is the difference in chemical potential relative to that at coexistence, $\Delta\mu > 0$ represents gas–liquid nucleation and $\Delta\mu < 0$ represents liquid–gas nucleation. ρ_{l0} and ρ_{v0} are the bulk densities of the liquid and the vapour at coexistence, and ρ_m is the intersection of two parabolae given by

$$\rho_m = \rho_{v0} + (\lambda/2\lambda_v)\,\Delta\rho = \rho_{l0} - (\lambda/2\lambda_l)\,\Delta\rho \tag{2.7}$$

where

$$\lambda/2 = \lambda_l\lambda_v/(\lambda_l + \lambda_v)$$

$$\Delta\rho = \rho_{l0} - \rho_{v0}.$$

λ_l and λ_v are the inverses of the bulk correlation lengths of liquid and vapour and are proportional to the bulk isothermal compressibility of each phase. When $\Delta\mu \neq 0$, the equilibrium liquid density ρ_l and equilibrium vapour density ρ_v differ from those at coexistence, namely ρ_{l0} and ρ_{v0}, and are given by

$$\begin{aligned} \rho_l &= \rho_{l0} + \Delta\mu/\lambda_l^2 \\ \rho_v &= \rho_{v0} + \Delta\mu/\lambda_v^2. \end{aligned} \tag{2.8}$$

Hence, ρ_b in equations (2.1) and (2.4) are

$$\rho_b = \begin{cases} \rho_v & \text{gas–liquid nucleation} \\ \rho_l & \text{liquid–gas nucleation.} \end{cases}$$

The difference $L\,\Delta p$ between the liquid and vapour pressures appearing in equations (1.2)–(1.4), *namely*

$$L\,\Delta p = \omega(\rho_l) - \omega(\rho_v)$$

is written as

$$\Delta p = \Delta\mu\,\Delta\rho + \tfrac{1}{2}(\Delta\mu)^2(1/\lambda_l^2 - 1/\lambda_v^2). \tag{2.9}$$

Of course, when $\Delta\mu = 0$, we have $\Delta p = 0$.

The critical point cannot be simulated properly by this double-parabola model, but the spinodal point [11] can be defined formally as the points where $\rho_m = \rho_v$ or $\rho_m = \rho_l$, for which the chemical potential $\Delta\mu_v$ (gas spinodal) and $\Delta\mu_l$ (liquid spinodal) are given by

$$\begin{aligned} \Delta\mu_v &= \tfrac{1}{2}\lambda\lambda_v\,\Delta\rho \qquad (\rho_m = \rho_v, \text{ gas spinodal}) \\ \Delta\mu_l &= -\tfrac{1}{2}\lambda\lambda_l\,\Delta\rho \qquad (\rho_m = \rho_v, \text{ liquid spinodal}). \end{aligned} \tag{2.10}$$

As pointed out by Oxtoby and Evans [7] for the hard-sphere van der Waals model, the absolute value of $\Delta\mu_v$ at the gas spinodal is greater than $\Delta\mu_l$ at the liquid spinodal since $\lambda_v > \lambda_l$ in general. When $\Delta\mu < 0$, this double-parabola model has the singularity $\Delta p = 0$ at

$$\Delta\mu_c = -\lambda\,\Delta\rho/(1/\lambda_l + 1/\lambda_v) \tag{2.11}$$

which is located in the unphysical region beyond the spinodal point $\Delta\mu_l$.

The analytic solutions of the differential equation (2.3) which satisfy the boundary conditions (2.5) are easily obtained for the model potential (2.6).

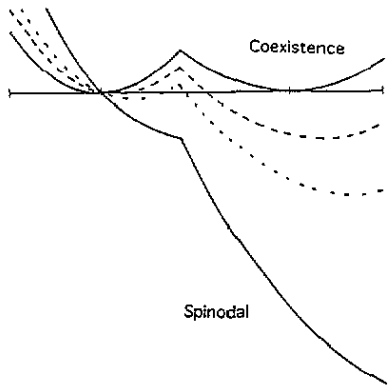

Figure 1. The free-energy density $\omega(\rho)$ of a uniform fluid. Note that the curves have a typical double-minimum form. The unstable minimum with higher energy loses local stability at the spinodal.

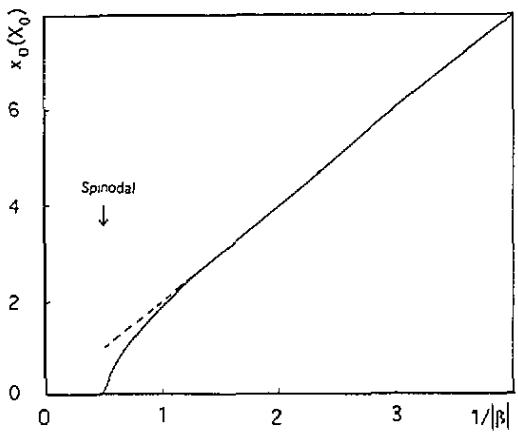

Figure 2. The classical (– – –) and the non-classical (——) critical radii of a nucleus (liquid or vapour) as functions of the degree $1/|\beta|$ of supersaturation when $\alpha = 1$ (symmetrical fluid). They are roughly linear in $1/|\beta|$. Note that in this case the curves represent both vapour–liquid and liquid–vapour critical radii because of symmetry. The non-classical radius approaches zero while the classical radius approaches a finite value at the spinodal.

2.1. *Gas–liquid nucleation* ($\Delta\mu > 0$)

$$\rho(r) = \begin{cases} \rho_l - (r_0/r)L_l \operatorname{cosech}(\lambda_l r_0)\sinh(\lambda_l r) & r < r_0 \\ \rho_v + (r_0/r)L_v \exp[-\lambda_v(r - r_0)] & r > r_0. \end{cases} \tag{2.12}$$

The amplitudes of density variation are

$$\begin{aligned} L_l &= (\lambda/2\lambda_l)\,\Delta\rho + \Delta\mu/\lambda_l^2 = \rho_l - \rho_m \\ L_v &= (\lambda/2\lambda_v)\,\Delta\rho - \Delta\mu/\lambda_v^2 = \rho_m - \rho_v. \end{aligned} \tag{2.13}$$

The 'non-classical' radius r_0 of the critical droplet, which corresponds to the 'classical' radius R_0 in equation (1.3), is determined from the continuity of the first derivative of the

density profile $d\rho(r)/dr$ at r_0 and is the solution of the equation

$$(1 + L_v/L_l) + L_v\lambda_v/L_l\lambda_l(\lambda_l r_0) = (\lambda_l r_0)\coth(\lambda_l r_0) \tag{2.14}$$

which has a unique solution r_0 when $\Delta\mu > 0$ and $r_0 \to \infty$ as $\Delta\mu \to 0^+$. Using equation (2.13), equation (2.14) can be transformed into

$$\rho_m/\rho_l = \{1 - [1 - (\rho_v/\rho_l)(1 + \lambda_v r_0)](1/\lambda_l r_0)\tanh(\lambda_l r_0)\}/[1 + (\lambda_v/\lambda_l)\tanh(\lambda_l r_0)]$$

which is used by Oxtoby (by setting $\rho_v = 0$) in a similar double-parabola model of crystal-melt nucleation [18]. An almost equivalent model has also been used by Holyst and Poniewierski [17] to discuss the wetting on a sphere.

Using the density profiles (2.12), the non-classical barrier height $\Delta\Omega_{ncl}$ corresponding to the classical barrier height $\Delta\Omega_{cl}$ in equation (1.4) can be calculated from equation (2.1) as

$$\Delta\Omega_{ncl} = -\tfrac{4}{3}\pi r_0^3 L\,\Delta p + (2\pi L L_l^2/\lambda_l)[\lambda_l r_0\,\mathrm{cosech}(\lambda_l r_0)]^2 F(\lambda_l r_0)$$
$$+ (2\pi L L_v^2/\lambda_v)[\lambda_v r_0 \exp(\lambda_v r_0)]^2 G(\lambda_v r_0)$$

where

$$F(x) = (-1 - \exp(4x) + x\exp(4x) - x + 2\exp(2x))/4x\exp(2x)$$
$$G(x) = [(1 + x)\exp(-2x)]/x$$

which, using equation (2.14), can be further simplified to [18]

$$\Delta\Omega_{ncl} = -\tfrac{4}{3}\pi r_0^3 L\,\Delta p + 2\pi L(\rho_m - \rho_v)(\rho_l - \rho_v)r_0(1 + \lambda_v r_0). \tag{2.15}$$

Then, the surface free energy γ' of the spherical droplet with radius r_0, which corresponds to the surface tension γ of the planar interface at coexistence, is given by

$$\gamma' = (L/2r_0)(\rho_m - \rho_v)(\rho_l - \rho_v)(1 + \lambda_v r_0) \tag{2.16}$$

where r_0 is determined through equation (2.14) as a function of $\Delta\mu$. Since $r_0 \to \infty$ as $\Delta\mu \to 0^+$, $\gamma'(\Delta\mu \to 0^+)$ coincides with the surface tension of the planar interface:

$$\gamma = \tfrac{1}{4}L\lambda(\Delta\rho)^2 \tag{2.17}$$

at coexistence $\Delta\mu = 0$ of this double-parabola model. Inserting equations (2.9) and (2.17) into equations (1.3) and (1.4), we can calculate the radius r_0 and the barrier height $\Delta\Omega_{cl}$ of the critical droplet from the classical 'capillarity approximation'; the results will be reported in the next section.

2.2. Liquid–gas nucleation ($\Delta\mu < 0$)

In this case, we can obtain the solutions by replacing $\lambda_l \to \lambda_v$, $\lambda_v \to \lambda_l$, and $\Delta\rho \to -\Delta\rho$, i.e. $L_v \to -L_l$ and $L_l \to -L_v$ in those of gas–liquid nucleation. The density profile, for example, becomes

$$\rho(r) = \begin{cases} \rho_v + (r_0/r)L_v \operatorname{cosech}(\lambda_v r_0)\sinh(\lambda_v r) & r < r_0 \\ \rho_l - (r_0/r)L_l \exp[-\lambda_l(r - r_0)] & r > r_0. \end{cases} \tag{2.18}$$

The critical radius r_0 of the 'critical bubble' is determined from

$$(1 + L_l/L_v) + (L_l\lambda_l/L_v\lambda_v)(\lambda_v r_0) = (\lambda_v r_0)\coth(\lambda_v r_0). \tag{2.19}$$

This equation has a single solution r_0 so long as $\Delta\mu < 0$, and again $r_0 \to \infty$ as $\Delta\mu \to 0^-$.

Using the density profile (2.18), we can calculate the barrier height as

$$\Delta\Omega_{ncl} = +\tfrac{4}{3}\pi r_0^3 L\,\Delta p + 2\pi L(\rho_l - \rho_m)(\rho_l - \rho_v)r_0(1 + \lambda_l r_0) \tag{2.20}$$

which should be compared with equation (2.15); however, $\Delta\mu < 0$ in this case and, hence, $\Delta p < 0$. Again, we can define the surface free energy of the bubble as equation (2.16), which is also equal to the surface tension of the planar interface (2.17) in the limit $\Delta\mu \to 0^-$.

All the above results are expressed as functions of the supersaturation measured by $\Delta\mu$, and λ_l, λ_v and $\Delta\rho$ which characterize the bulk thermodynamics. The numerical results will be presented in the next section.

3. Results

The above results can be characterized, in fact, by only two parameters if we use appropriate scaling of variables. We introduce the parameter α which represents the asymmetry of the thermodynamics properties of the liquid and vapour phases, and β instead of $\Delta\mu$ which is the deviation of the chemical potential from coexistence:

$$\begin{aligned} &\alpha = \lambda_l/\lambda_v \\ &\beta = (4\,\Delta\mu)/(\lambda^2\,\Delta\rho). \end{aligned} \tag{3.1}$$

Here β is proportional to $\Delta\mu$ and represents the shift in equilibrium density relative to that at coexistence as we can anticipate from equation (2.8). Since $\lambda_v > \lambda_l$ in general, the asymmetry $\alpha < 1$. We term a fluid with $\alpha = 1$ a symmetric fluid and a fluid with $\alpha < 1$ an asymmetric fluid. Similarly, we introduce the scaled quantities

$$\begin{aligned} &\lambda_l r \longrightarrow x \\ &\lambda_v r \longrightarrow y(= x/\alpha) \\ &(\rho(r) - \rho_{v0})/\Delta\rho \longrightarrow \tilde{\rho}(x) \text{ or } \tilde{\rho}(y) \\ &\Delta\Omega[\rho]/(4\pi L\,\Delta\rho^2/3\lambda) \longrightarrow \Delta\tilde{\Omega}[\tilde{\rho}]. \end{aligned} \tag{3.2}$$

Then the results of the previous section are as follows.

3.1. Gas–liquid nucleation ($\beta > 0$)

The density profile (2.12) *is now written as*

$$\tilde{\rho}(x) = \begin{cases} 1 + [\beta/(1+\alpha)^2] - [(1+\alpha+\beta)/(1+\alpha)^2](x_0/x)\,\mathrm{cosech}(x_0)\sinh(x) \\ \qquad x < x_0 \\ [\alpha^2/(1+\alpha)^2]\beta + [\alpha(1+\alpha-\alpha\beta)/(1+\alpha)^2](y_0/y)\exp[-(y-y_0)] \\ \qquad y > y_0. \end{cases} \tag{3.3}$$

Equation (2.14), which determines the 'non-classical' radius $x_0 = \lambda_l r_0$ or $y_0 = \lambda_v r_0$, becomes

$$[1 + \alpha(1+\alpha-\alpha\beta)/(1+\alpha+\beta)] + [(1+\alpha-\alpha\beta)/(1+\alpha+\beta)]x_0 = x_0\coth(x_0). \tag{3.4}$$

Since the equilibrium densities (2.8) at $\Delta\mu$ scaled by equation (3.2) are given by

$$\tilde{\rho}_l = 1 + \beta/(1+\alpha)^2$$
$$\tilde{\rho}_v = \beta\alpha^2/(1+\alpha)^2$$

then the density at the centre of the critical nucleus is

$$\tilde{\rho}(0) = \tilde{\rho}_l - [(1+\alpha+\beta)/(1+\alpha)^2][x_0/\sinh(x_0)]$$

which is always lower than the equilibrium density $\tilde{\rho}_l$ at the chemical potential $\Delta\mu$. *Similarly, the non-classical surface free energy* γ' *(equation* (2.16)*) divided by the surface tension* γ *of the planar interface (equation* (2.17)*) is written as*

$$\gamma'/\gamma = (1/y_0)[(1+\alpha-\alpha\beta)(1+\alpha+\beta-\alpha\beta)/(1+\alpha)^2](1+y_0) \tag{3.5}$$

where $y_0 (= x_0/\alpha)$ is determined from equation (3.4). This ratio approaches unity as $\beta \to 0^+$ since $x_0 \to \infty$.

The non-classical energy barrier $\Delta\tilde{\Omega}_{ncl}$ corresponding to equation (2.15) can be expressed as a function of α, β and x_0, but we shall not reproduce the result.

3.2. Liquid-gas nucleation ($\beta < 0$)

In this case, we can obtain the equations by simply replacing $\alpha \to 1/\alpha$, $\beta \to -\beta$, $y \to x$, $x \to y$ and $\tilde{\rho} \to 1 - \tilde{\rho}$ in those for gas–liquid nucleation, and the density profile of the bubble, for example, becomes

$$\tilde{\rho}(x) = \begin{cases} \alpha^2\beta/(1+\alpha)^2 + [\alpha(1+\alpha-\alpha\beta)/(1+\alpha)^2](y_0/y)\,\mathrm{cosech}(y_0)\sinh(y) \\ \qquad y < y_0 \\ 1 + \beta/(1+\alpha)^2 - [(1+\alpha+\beta)/(1+\alpha)^2](x_0/x)\exp[-(x-x_0)] \\ \qquad x > x_0. \end{cases} \tag{3.6}$$

Equation (2.19), which determines the radius $x_0 = \lambda_l r_0$ and $y_0 = \lambda_v r_0$ of the critical bubble, now becomes

$$[1 + (1+\alpha+\beta)/\alpha(1+\alpha-\alpha\beta)] + [(1+\alpha+\beta)/(1+\alpha-\alpha\beta)]y_0 = y_0\coth(y_0) \tag{3.7}$$

and the vapour density at the centre of the bubble is

$$\tilde{\rho}(0) = \tilde{\rho}_v + [\alpha(1+\alpha-\alpha\beta)/(1+\alpha)^2][y_0/\sinh(y_0)]$$

which is always higher than $\tilde{\rho}_v$ at the chemical potential $\Delta\mu$. One may also derive expressions for the surface free energy and the barrier height as a function of α, β and x_0.

Comparing equations (3.4) and (3.7), we observe that for a symmetric fluid with $\alpha = 1$ the critical radii of the liquid droplet from equation (3.4) and the vapour bubble from equation (3.7) calculated at the same degree $|\beta|(|\Delta\mu|)$ of supersaturation are equal. In general, however, they are different for the same degree $|\Delta\mu|$ of supersaturation because $\alpha < 1$. Both equation (3.4) and equation (3.7) predict a diverging radius, i.e.

$$x_0 \to (1+\alpha)/|\beta| \qquad \text{as} \qquad |\beta| \to 0 \tag{3.8}$$

as demonstrated by Cahn and Hilliard [11], and vanishing radii, i.e.

$$x_0 = y_0 = 0$$

at $\beta_v = (1+\alpha)/\alpha$ and $\beta_l = -(1+\alpha)$ corresponding to $\Delta\mu_v$ (vapour spinodal) and $\Delta\mu_l$ (liquid spinodal). Although these vanishing radii contradict the conclusion of Cahn and Hilliard [11], who predicted diverging radii, it is due to the difference between the definition of radius in our model and the definition in theirs. In fact, as spinodals are approached, the density profile becomes more and more vapour like for liquid–vapour nucleation as one can see from equations (3.3), and liquid like for vapour–liquid nucleation from equations (3.6), and they both approach a constant density $\alpha/(1+\alpha)$, which is qualitatively the same behaviour as observed by Cahn and Hilliard [11].

The classical radius $X_0 = \lambda_l R_0$ is, using equations (1.3), (2.9) and (2.17), written as

$$X_0 = (1+\alpha)/|\beta + 2\beta^2(1-\alpha)/(1+\alpha)| \tag{3.9}$$

which has the same limiting form as the non-classical results (3.8) when $|\beta| \to 0$ or $\alpha = 1$. Even the classical radii of the liquid and the vapour nuclei are different for the same $|\beta|$ when $\alpha \neq 1$.

In figure 2, we have plotted 'classical' and 'non-classical' critical radii X_0 and x_0 as functions of supersaturation $\beta(\propto \Delta\mu)$ for a symmetric ($\alpha = 1$) fluid. In this case the gas–liquid nucleation and the liquid–gas nucleation are completely symmetric; the magnitudes of critical radii are equal for the same degree $|\beta|$ of supersaturation. We have to note that $\beta < 0$ corresponds to bubble formation and $\beta > 0$ to droplet formation. Both classical and non-classical radii are roughly linear in $1/|\beta|$ as one can expect from equation (3.9). The deviations of the non-classical radius from the classical radius are only appreciable near the spinodals.

The critical radii for an asymmetric fluid with $\alpha = 0.7$ are shown in figure 3. A singular tendency observed in the classical result when we approach the (liquid) spinodal point β_l is due to the unphysical singularity at $\beta_c = -2(1+\alpha)/(1-\alpha)$ corresponding to $\Delta\mu_c$ in equation (2.11), which is certainly an artefact of the simplicity of this double-parabola model. As we can observe from the figure, the deviations in the magnitude of the non-classical radius from the classical radius become larger as the asymmetry is increased (α decreased); the non-classical radius is larger, on the whole, than the classical radius for liquid droplet formation and, on the other hand, the classical radius is always larger than

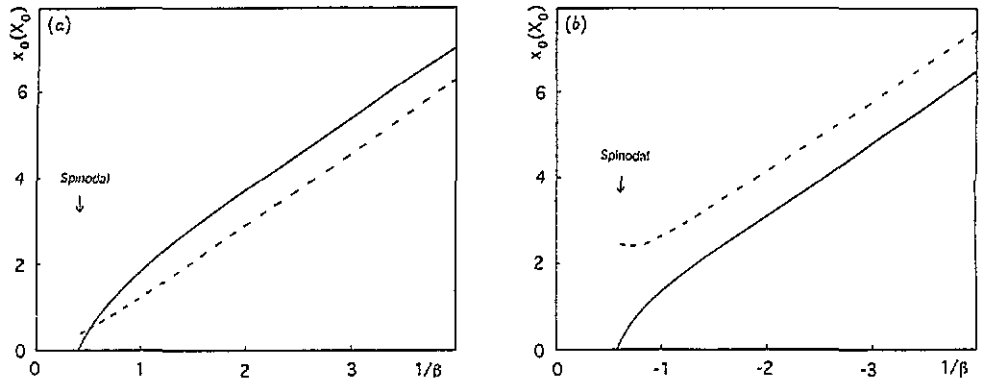

Figure 3. (*a*) The same as in figure 2, but for droplet formation (vapour–liquid nucleation) when $\alpha = 0.7$. The non-classical radius is on the whole greater than the classical radius.(*b*) The same as in (*a*), but for bubble formation (liquid–vapour nucleation). Now, the non-classical radius is always smaller than the classical radius, and the difference is larger than that for droplet formation.

the non-classical radius for vapour bubble formation, and the non-classical effect is more pronounced in liquid–vapour nucleation (cavitation) than in vapour–liquid nucleation. These results are qualitatively in accord with the numerical results of Oxtoby and Evans [7].

The typical density profiles of the droplet and the bubble are displayed in figure 4 for various degrees β of supersaturation and asymmetry $\alpha = 0.7$. The densities of the liquid and the vapour at coexistence are unity and zero on the scale (3.2); the density at the centre of the liquid nucleus is higher than the liquid density of unity at coexistence when β is small, but eventually it becomes lower as the spinodal $\beta_v \simeq 2.43$ is approached. The density at the centre of a vapour bubble is lower than the vapour density of zero at coexistence but it becomes higher as the liquid spinodal $\beta_l = 1.7$ is approached. Clearly, as noted in the previous paragraph, both densities approach $0.7/1.7 \simeq 0.4$ at the spinodals for $\alpha = 0.7$. Again, as one can anticipate from figure 3, the non-classical effect on the density profile is more pronounced in liquid–vapour nucleation (bubble formation).

In figure 5 we have plotted the ratio of the surface free energy of the nucleus divided by the surface tension of the planar interface given by equation (3.5) for $\beta > 0$ and by a similar equation for $\beta < 0$. We have already pointed out that this ratio approaches unity in the limit of low supersaturation $\beta \to 0$. It reaches a maximum larger than unity somewhere and then starts to decrease to zero as β increases from zero to the vapour spinodal in vapour–liquid nucleation $\beta > 0$; this maximum is higher and the region where it exceeds unity (surface free energy of the spherical droplet is greater than the planar surface free energy) is wider as the asymmetry is increased (α decreased). An effective surface tension γ' of a small spherical droplet with large β is smaller than the surface tension of a planar interface because $\gamma'/\gamma < 1$. A similar behaviour of the surface free energy of the droplet has been observed by several workers [19, 20]. For bubble formation ($\beta < 0$), this ratio is always smaller than unity and monotonically decreases to zero at the liquid spinodal, and the deviation of γ' from γ is again larger as the asymmetry is increased. This different and asymmetrical behaviour of the surface free energy of the droplet and the bubble affects the free-energy barrier height of nucleation, which we shall discuss next.

In figures 6 and 7 we have plotted the classical free energy barrier height $\Delta\tilde{\Omega}_{cl}$ and the non-classical free energy barrier height $\Delta\tilde{\Omega}_{ncl}$ as functions of $\beta^{-2}(\propto \Delta\mu^{-2})$. The

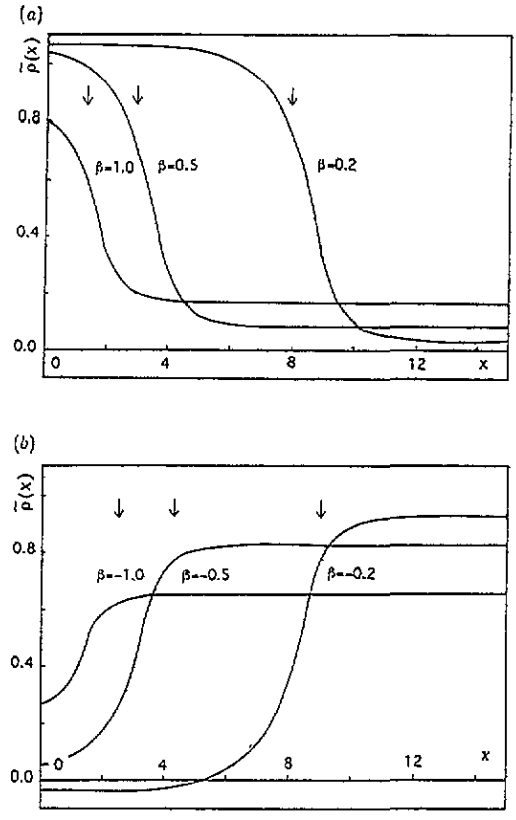

Figure 4. (*a*) Typical density profiles of a droplet with asymmetry $\alpha = 0.7$ for several values of the supersaturation β. The arrows indicate the classical radii calculated from equation (3.9), which seem a good estimate of the size of the droplet. (*b*) The same as in (*a*) but for bubble formation. The real density profiles are measurably shrunk from those expected from the classical radii indicated by arrows. The non-classical effect is more appreciable in bubble formation than in droplet formation in (*a*).

classical barrier height is calculated from equations (2.9) and (2.17), which becomes, using the scaling (3.2)

$$\Delta\tilde{\Omega}_{\rm cl} = \beta^{-2}/\{1 + (\beta/2)[(1-\alpha)/(1+\alpha)]\}^2 \tag{3.10}$$

from which we expect that the barrier height is roughly linear in β^{-2}. The barrier height for a symmetric fluid with $\alpha = 1$ is plotted in figure 6. In this case, liquid–vapour and vapour–liquid nucleation are symmetric, the barrier heights always satisfy $\Delta\Omega_{\rm cl} > \Delta\Omega_{\rm ncl}$, and the non-classical nucleation rate will be always faster than the classical nucleation rate if we calculate the classical and non-classical nucleation rates $J_{\rm cl}$ and $J_{\rm ncl}$ from equation (1.1) using the barrier heights $\Delta\Omega_{\rm cl}$ and $\Delta\Omega_{\rm ncl}$.

A more realistic case of an asymmetric fluid with $\alpha = 0.7$ is displayed in figure 7. The non-classical and the classical barrier heights cross at some point (figure 7(*a*)) for liquid droplet formation ($\beta > 0$). Therefore, the crossing indicates that, for small supersaturation β, the non-classical nucleation rate will be slower than the classical nucleation rate ($J_{\rm cl} > J_{\rm ncl}$) because $\Delta\Omega_{\rm ncl} > \Delta\Omega_{\rm cl}$ while $J_{\rm ncl} > J_{\rm cl}$ for sufficiently large β. Oxtoby and Evans [7] argued that for parameters appropriate to real materials it happens that

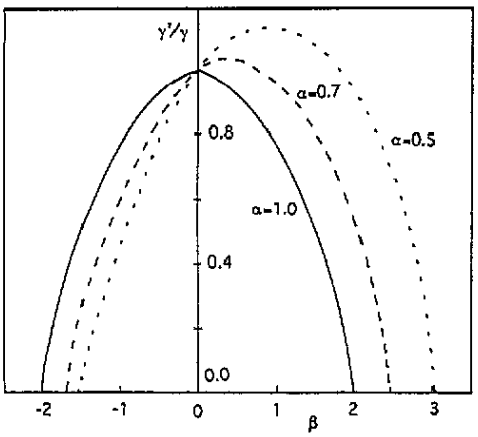

Figure 5. The surface free energy γ' of a nucleus divided by the surface tension γ of the planar interface. The negative $\beta < 0$ represents bubble formation and positive $\beta > 0$ droplet formation. The ratio γ'/γ approaches unity at $\beta = 0$ and zero at spinodals. The curve is symmetrical for a symmetric fluid with $\alpha = 1$. Note that the curve exceeds the ratio of unity in some interval when a fluid is asymmetric.

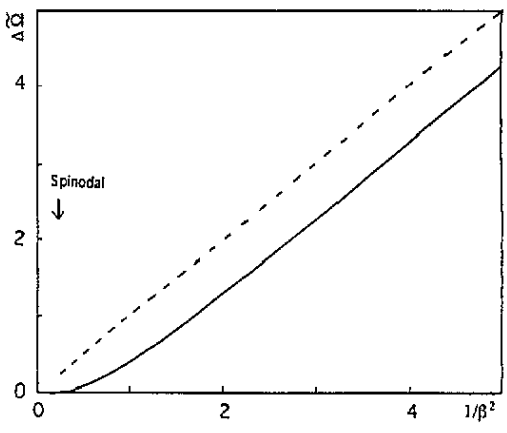

Figure 6. The nucleation free-energy barrier height of classical (– – –) and non-classical (——) theories for a symmetric fluid with $\alpha = 1$. Note that in this case the curves represent both droplet formation and bubble formation. The non-classical barrier height is always lower than the classical barrier height, which suggests a faster non-classical nucleation rate than a classical nucleation rate.

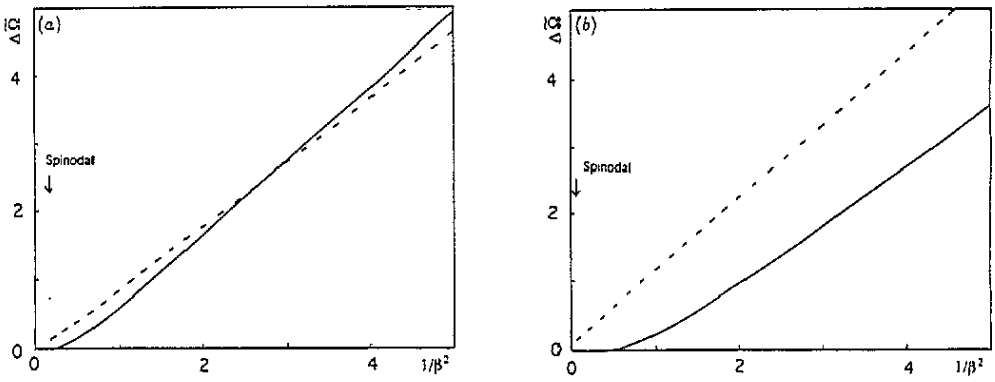

Figure 7. (*a*) The same as figure 6, but with $\alpha = 0.7$ and for droplet formation. In this case, two curves cross at some point, where the classical and the non-classical nucleation rates have the same magnitude; the non-classical effect could be small for the vapour–liquid nucleation. (*b*) The same as in (*a*) but for bubble formation. This figure is similar to figure 6, but now the deviations of the non-classical barrier heights from the classical barrier heights are large, which suggests a large non-classical effect on the liquid–vapour nucleation rate.

$\Delta\Omega_{\rm cl} \simeq \Delta\Omega_{\rm ncl}$ and, hence, $J_{\rm cl} \simeq J_{\rm ncl}$, which is the reason why the classical nucleation theory has been satisfactory so far; the success of classical theory occurs just by chance!

The energy barrier for bubble formation is quite different (figure 7(*b*)), in contrast with droplet formation, reflecting a different behaviour of the surface free energy (figure 5(*b*)). It always satisfies $\Delta\Omega_{\rm cl} > \Delta\Omega_{\rm ncl}$, and the difference between the classical and the non-classical barriers is much greater than that for droplet formation (figure 7(*a*)), by which we may expect a much faster non-classical nucleation rate $J_{\rm ncl} \gg J_{\rm cl}$. Such a large non-classical

effect has already been predicted from numerical work [7, 9] and suggests the possibility of detecting a non-classical effect in liquid–vapour bubble formation. It is also obvious from figure 7(*b*) that such a large non-classical effect is more easily detectable in materials with a large asymmetry (small α).

Because of the simplicity of this double-parabola model, temperature effects are not expected to be handled properly, especially near the critical point. Furthermore, various parameters are temperature dependent, which makes the application of this analysis to the temperature effects more difficult. For example, the asymmetry α depends strongly on temperature. From the theoretical estimation of the bulk correlation lengths λ_l and λ_v for a series of temperatures in the literature [12], we find that α depends almost linearly on temperature; it starts from a very small value at a low temperature and linearly increases and approaches unity (symmetric fluid) at the critical point. One might naively expect, at most, that the non-classical effects will be pronounced at low temperatures because of small α and large asymmetry.

Finally, we close this section by estimating the magnitude of the non-classical effect on the nucleation rate numerically. From equation (1.1), the non-classical nucleation rate J_{ncl} divided by the classical nucleation rate J_{cl} becomes

$$J_{ncl}/J_{cl} = \exp[(\Delta\Omega_{cl} - \Delta\Omega_{ncl})/k_BT] \simeq \exp\{\tfrac{4}{3}\pi[(\rho_l/\lambda_l^3)/(\rho_l k_B T\kappa_l)](\Delta\tilde{\Omega}_{cl} - \Delta\tilde{\Omega}_{ncl})\}$$

where we have considered a relatively low temperature and used the scaling (3.2), $L\lambda_l^2 \sim (\rho_l^2\kappa_l)^{-1}$, where κ_l is the isothermal compressibility of bulk liquid, $\Delta\rho \sim \rho_l$, and $\lambda \sim \lambda_l$ to eliminate L. If we consider a standard monatomic fluid with atomic diameter d, the bulk correlation length is given by $\lambda_l^{-1} \sim d$ and $\rho_l \sim 6\eta/\pi d^3$ with $\eta \simeq 0.5$, the packing fraction from standard liquid state theory; then we have

$$J_{ncl}/J_{cl} \simeq \exp[(4/\rho_l k_B T\kappa_l)(\Delta\tilde{\Omega}_{cl} - \Delta\tilde{\Omega}_{ncl})].$$

A typical magnitude of the normalized isothermal compressibility is $\rho_l k_B T\kappa_l \simeq 0.1$ [7]; therefore,

$$J_{ncl}/J_{cl} \sim \exp[40(\Delta\tilde{\Omega}_{cl} - \Delta\tilde{\Omega}_{ncl})]. \tag{3.11}$$

From figure 7(*a*), $\Delta\tilde{\Omega}_{cl} - \Delta\tilde{\Omega}_{ncl} \simeq +0.2$—$0.2$ for vapour–liquid nucleation when the degree of asymmetry is $\alpha = 0.7$; therefore, $J_{ncl}/J_{cl} \simeq 10^{+4}$–$10^{-4}$. On the other hand, for cavitation, we have from figure 7(*b*) that $\Delta\tilde{\Omega}_{cl} - \Delta\tilde{\Omega}_{ncl} \simeq +0.5$—$+1.0$; therefore, $J_{ncl}/J_{cl} \simeq 10^{+9}$–$10^{+18}$; the non-classical rate is always faster than the classical rate, and the deviation amounts to between nine and 18 orders of magnitude. Such a huge non-classical effect on liquid–vapour nucleation (cavitation) has already been predicted numerically by Oxtoby and co-workers [7, 9], and we reconfirm their result. It is again obvious that the non-classical effect is more marked for smaller α and larger asymmetry.

4. Conclusions

In this paper we have calculated the barrier height and the density profile of the nucleus for homogeneous nucleation using the 'non-classical' Cahn–Hilliard theory without using the so-called 'classical' capillarity approximation and by employing the double-parabola model and the square-gradient approximation. Most of our results are common to those obtained by Oxtoby and Evans [7] using a similar non-classical theory; however, our analysis clearly

demonstrated that asymmetry of the bulk thermodynamics of liquid and vapour phases plays a crucial role in producing non-classical effects, which, in particular, could be huge for bubble formation in liquids under tensile stress (cavitation). Although the double-parabola model is so simple that parameters other than asymmetry represented by the ratio of the compressibilities could equally play a crucial role in reality, it will be interesting to observe such non-classical effects experimentally in cavitation in such materials with a large asymmetry or at a low temperature far from the critical point where the asymmetry is more pronounced.

Finally, we note that, although we have used a local density-functional theory based on the square-gradient approximation, the final results will not be altered qualitatively even if we use a non-local density-functional theory as long as the intermolecular force remains short ranged and will be even semiquantitatively correct by an appropriate renormalization of the correlation length [12]. For a special type of integration kernel with exponential form, the integral equation derived from non-local density functional is solvable analytically [21, 22], and an almost parallel analysis to this work may be possible. We believe, finally, that this work is of use in understanding the qualitative aspects of liquid–solid nucleation [23] as well. Very recently, Oxtoby [18] initiated use of a similar double-parabola model to study the liquid–solid problem.

Acknowledgment

The author is grateful to Professor David W Oxtoby (University of Chicago) for illuminating comments and sending [18], which also suggested a simpler formula (2.15).

References

[1] Oxtoby D W 1992 *J. Phys.: Condens. Matter* **4** 7627
[2] Oxtoby D W 1992 *Fundamentals of Inhomogeneous Fluids* ed D Henderson (New York: Dekker) ch 10
[3] Volmer M and Weber A 1926 *Z. Phys. Chem.* **119** 277
[4] Becker R and Döring W 1935 *Ann. Phys., Lpz.* **24** 719
[5] Zeldvich J 1942 *Sov. Phys.–JETP* **12** 525
[6] Langer J S and Turski L A 1973 *Phys. Rev.* A **8** 3230
[7] Oxtoby D W and Evans R 1988 *J. Chem. Phys.* **89** 7521
[8] Zettlemoyer A C (ed) 1955 *Nucleation* (New York: Dekker)
[9] Zeng X C and Oxtoby D W 1991 *J. Chem. Phys.* **94** 4472
[10] Hung C, Krasnopoler M J and Katz J L 1989 *J. Chem. Phys.* **90** 1858
[11] Cahn J W and Hilliard J E 1959 *J. Chem. Phys.* **31** 688
[12] Lu B Q, Evans R and Telo da Gama M M 1985 *Mol. Phys.* **55** 1319
[13] Rowlinson J S and Widom B 1982 *Molecular Theory of Capillarity* (Oxford: Oxford University Press)
[14] Evans R 1979 *Adv. Phys.* **28** 143
[15] Hauge E H 1986 *Phys. Rev.* B **33** 3322
[16] Stovneng J A, Aukrust T and Hauge E H 1987 *Physica* A **143** 40
[17] Holyst R and Poniewierski A 1987 *Phys. Rev.* B **36** 5628
[18] Oxtoby D W 1993 *Phys. Scr.* at press
[19] Lee D J, Telo da Gama M M and Gubbins K E 1986 *J. Chem. Phys.* **85** 490
[20] Guermeur R, Biquard F and Jacolin C 1985 *J. Chem. Phys.* **82** 2040
[21] Sullivan D E 1981 *J. Chem. Phys.* **74** 2604
[22] Holyst R and Poniewierski A 1988 *Physica* A **149** 622
[23] Harrowell P and Oxtoby D W 1984 *J. Chem. Phys.* **80** 1639